THE METHOD OF FUNDAMENTAL SOLUTIONS IN SOLVING COUPLED BOUNDARY VALUE PROBLEMS FOR M/EEG

G. ALA*, G. FASSHAUER†, E. FRANCOMANO‡, S. GANCI*, AND M. MCCOURT§

Abstract. Estimation of neuronal activity in the human brain from electroencephalography (EEG) and magnetoencephalography (MEG) signals is a typical inverse problem whose solution process requires an accurate and fast forward solver. In this paper the Method of Fundamental Solution (MFS) is for the first time proposed as a truly meshfree, boundary-type, integration-free and easy to implement alternative to the Boundary Element Method (BEM) for solving the M/EEG forward problem. The solution of the forward problem is obtained, via the Method of Particular Solutions (MPS), by numerically solving a set of coupled boundary value problems for the 3D Laplace equation which has well behaved analytic fundamental solutions. Numerical accuracy, convergence, and computational load are investigated. The proposed method shows spectral convergence and is competitive with the state-of-the-art BEM.

Key words. kernel-based methods, method of fundamental solutions, EEG, MEG

AMS subject classifications. 35J25, 65Z05, 65N80, 92C55

1. Introduction.

The localization of neural activity is important both for diagnostic purpose and for neurophysiological research. As a consequence of the activation of a specific cortical area, i.e., a beam of neighboring neurons in the cerebral cortex, weak electrical currents flow in the brain giving rise to electric and magnetic fields. Electroencephalography (EEG) [1, 2] and magnetoencephalography (MEG) [3, 4] are completely non-invasive techniques for localizing the neural sources with a high time resolution by exploiting measurements of electric potential or magnetic field, respectively. However, these measurements do not provide direct information on the current distribution in the brain. To this end, a typical *inverse problem* has to be solved [5,6].

Given neural sources and head model, the evaluation of the electric potential or magnetic field at measuring points is the *forward problem*. Since the solution of an inverse problem requires many forward solves, a fast and accurate forward solver is needed.

So far, traditional mesh-based methods, such as the Finite Element Method (FEM) [7–9] and the Boundary Element Method (BEM) [10–13], have been used to address the M/EEG forward problem on domains generated by realistic head models [14]. Even though the former can handle the most realistic head models, the latter has become the method of choice and it is currently implemented in various widely used software packages for M/EEG source analysis [15, 16]. The success of the BEM is mainly due to its nature as a boundary-type method. Not only does it avoid very cumbersome and computationally expensive 3D mesh generation in the pre-processing stage, but it also has low computational cost when compared to the FEM for a given head model and numerical accuracy since it requires computational points only on the boundaries of the domain under investigation. However, the BEM still requires high quality meshing of the boundary manifolds, which is not a trivial task, involves costly numerical integration and could potentially introduce mesh-related artifacts

*DEIM, Università degli Studi di Palermo, Viale delle Scienze, ed. 9, Palermo, 90128, Italy
†Department of Applied Mathematics, Illinois Institute of Technology, Chicago, IL 60616, USA
‡DICGIM, Università degli Studi di Palermo, Viale delle Scienze, ed. 6, Palermo, 90128, Italy
§Department of Mathematical and Statistical Sciences, University of Colorado, Denver, CO 80202, USA

in the reconstructed neural activation patterns. Moreover, BEM suffers from slow convergence because of the use of low order polynomial approximations.

Difficulties in handling the geometrical complexity of biological structures motivated recent applications of meshfree methods in M/EEG research [17, 18]. However, the meshfree methods that have been proposed so far in this field, require computational nodes distributed in the entire domain. Therefore, though they avoid both the mesh generation step in pre-precessing and numerical integration, BEM may outperform them from a computational cost per accuracy standpoint, as shown in [17].

In this paper we propose, for the first time, the application of the Method of Fundamental Solutions (MFS) [19–22] for solving the coupled boundary value problems (BVPs) which arise in M/EEG forward solving.

The MFS approximates the solution of the given BVP by a linear combination of fundamental solutions of the governing partial differential equation (PDE). The coefficients of the linear combination are determined by enforcing it to satisfy the boundary conditions. Normals to boundaries and pairwise distances between points, are the only geometric quantities that are needed, so the MFS is truly meshfree. No numerical integration has to be performed, with remarkable savings in terms of computational cost with respect to BEM. For certain problems and for smooth data and domains, the MFS was proven to be spectrally convergent [23–25]. Further benefits come from the ease of implementation which makes computer codes very flexible as opposed to the BEM codes.

The outline of the paper is as follows. In Section 2 we present the formulation of the M/EEG forward problem. Section 3 deals with the MFS and its application to the M/EEG forward problem by means of the Method of Particular Solutions (MPS). In Section 4 we present simulation results for the EEG problem on simple geometries for which analytical or semi-analytical solutions are available. Comparisons with the state-of-the-art BEM demonstrate that the proposed method runs significantly faster than BEM, without sacrificing accuracy.

2. Problem Formulation.

It has been demonstrated that potential differences between points on the scalp and magnetic fields in the proximity of the head are mainly due to postsynaptic currents in apical dendrites of pyramidal neurons, which are perpendicular to the cortical surface and locally parallel to each other [26]. The activity of a beam of neighboring simultaneously-activated pyramidal neurons can be modeled by means of a current dipole [4, 27, 28]. On the basis of these assumptions, the M/EEG forward problem can be formulated by means of Maxwell's equations.

2.1. Maxwell's equations.

Let t be the time variable and $\boldsymbol{p}$ a point in a volume conductor domain $\Omega \subseteq \mathbb{R}^3$ with known and time-invariant, but spatially varying, conductivity $\sigma : \boldsymbol{p} \mapsto \sigma(\boldsymbol{p})$, electric permittivity $\epsilon : \boldsymbol{p} \mapsto \epsilon(\boldsymbol{p})$ and magnetic permeability $\mu : \boldsymbol{p} \mapsto \mu(\boldsymbol{p})$. Given a current density field $\mathbf{J} : (\boldsymbol{p}, t) \mapsto \mathbf{J}(\boldsymbol{p}, t)$ and a charge density $\rho : (\boldsymbol{p}, t) \mapsto \rho(\boldsymbol{p}, t)$ in Ω, the magnetic field $\mathbf{B} : (\boldsymbol{p}, t) \mapsto \mathbf{B}(\boldsymbol{p}, t)$, the electric field $\mathbf{E} : (\boldsymbol{p}, t) \mapsto \mathbf{E}(\boldsymbol{p}, t)$, the magnetizing field $\mathbf{H} : (\boldsymbol{p}, t) \mapsto \mathbf{H}(\boldsymbol{p}, t)$ and the displacement

field $\mathbf{D} : (\boldsymbol{p}, t) \mapsto \mathbf{D}(\boldsymbol{p}, t)$, can be evaluated by means of Maxwell's equations

$$\nabla \times \mathbf{E}(\boldsymbol{p}, t) = -\frac{\partial \mathbf{B}(\boldsymbol{p}, t)}{\partial t}, \tag{2.1a}$$

$$\nabla \times \mathbf{H}(\boldsymbol{p}, t) = \mathbf{J}(\boldsymbol{p}, t) + \frac{\partial \mathbf{D}(\boldsymbol{p}, t)}{\partial t}, \tag{2.1b}$$

$$\nabla \cdot \mathbf{D}(\boldsymbol{p}, t) = \rho(\boldsymbol{p}, t), \tag{2.1c}$$

$$\nabla \cdot \mathbf{B}(\boldsymbol{p}, t) = 0, \tag{2.1d}$$

with the constitutive relations

$$\mathbf{J}(\boldsymbol{p}, t) = \sigma(\boldsymbol{p})\mathbf{E}(\boldsymbol{p}, t), \tag{2.2a}$$

$$\mathbf{D}(\boldsymbol{p}, t) = \epsilon(\boldsymbol{p})\mathbf{E}(\boldsymbol{p}, t), \tag{2.2b}$$

$$\mathbf{B}(\boldsymbol{p}, t) = \mu(\boldsymbol{p})\mathbf{H}(\boldsymbol{p}, t). \tag{2.2c}$$

An application of the divergence operator to both sides of Equation (2.1b), taking into account Equation (2.1c), yields the continuity equation:

$$\nabla \cdot \mathbf{J}(\boldsymbol{p}, t) = -\frac{\partial \rho(\boldsymbol{p}, t)}{\partial t}. \tag{2.3}$$

2.2. The EEG forward problem. Since the maximum significant frequency in bio-electromagnetic phenomena is generally below 1 kHz and in light of the values of σ, ϵ and μ for typical biological tissues, the time dependence of all the above-mentioned equations can be neglected [3, 29]. As a result Equations (2.1) and Equation (2.3) turn out to be

$$\nabla \times \mathbf{E}(\boldsymbol{p}) = 0, \tag{2.4}$$

$$\nabla \times \mathbf{H}(\boldsymbol{p}) = \mathbf{J}(\boldsymbol{p}), \tag{2.5}$$

$$\nabla \cdot \mathbf{D}(\boldsymbol{p}) = 0, \tag{2.6}$$

$$\nabla \cdot \mathbf{B}(\boldsymbol{p}) = 0, \tag{2.7}$$

$$\nabla \cdot \mathbf{J}(\boldsymbol{p}) = 0, \tag{2.8}$$

respectively. Equation (2.4) suggests a direct consequence of the quasi-stationary approximation: the electric field is curl-free, therefore it can be expressed through the gradient of a scalar potential ϕ, namely the electric potential, as follows:

$$\mathbf{E}(\boldsymbol{p}) = -\nabla\phi(\boldsymbol{p}). \tag{2.9}$$

It is convenient to express the current density field as the sum of the source (impressed) current density $\mathbf{J}_s(\boldsymbol{p})$ and the volume current density given by $\mathbf{J}_\Omega(\boldsymbol{p}) = \sigma(\boldsymbol{p})\mathbf{E}(\boldsymbol{p}) = -\sigma(\boldsymbol{p})\nabla\phi(\boldsymbol{p})$, i.e.,

$$\mathbf{J}(\boldsymbol{p}) = \mathbf{J}_s(\boldsymbol{p}) - \sigma(\boldsymbol{p})\nabla\phi(\boldsymbol{p}). \tag{2.10}$$

Then, by considering Equation (2.10), the continuity equation (2.8) provides a relationship between the unknown potential and the given current source:

$$\nabla \cdot (\sigma(\boldsymbol{p})\nabla\phi(\boldsymbol{p})) = \nabla \cdot \mathbf{J}_s(\boldsymbol{p}). \tag{2.11}$$

With proper boundary conditions, Equation (2.11) can be solved analytically for special cases or numerically for realistic geometries. It can be shown that both Neumann and Dirichlet boundary conditions have to be imposed. In fact, in order to satisfy equations (2.8) and (2.4), the normal component of the current density and the potential, respectively, have to be continuous across interfaces between different media.

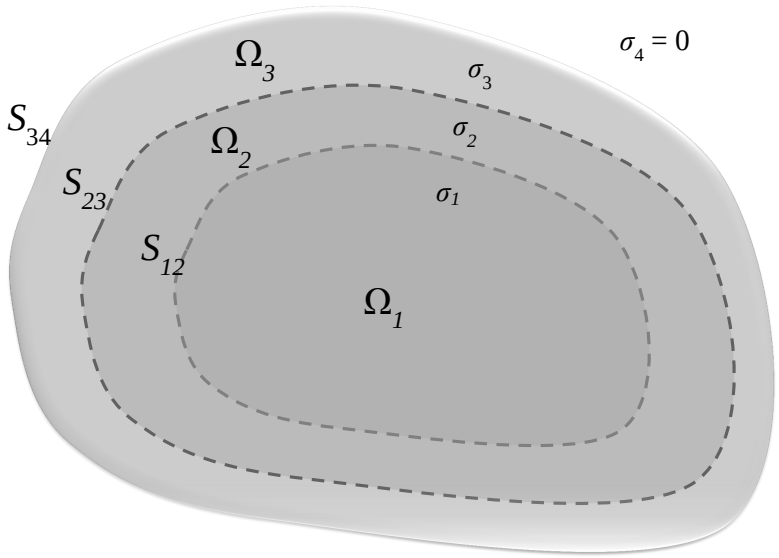

FIG. 2.1. *Piecewise-constant conductivity head model with nested regions - EDIT THIS FIGURE (symbols etc) Yup!*

2.3. Coupled boundary value problems. We concentrate our attention on the common piecewise-constant conductivity head model with nested regions, as shown in Figure 2.1. However, generalization to other topologies is straightforward (see Section 3 for an example). Let L be the number of regions in the domain Ω that represents the head, Ω_ℓ be the generic region, with boundary $\partial\Omega_\ell$ and conductivity σ_ℓ, and let $\mathcal{I}_{\ell,\ell+1} = \partial\Omega_\ell \cap \partial\Omega_{\ell+1}$ be the interface between the region ℓ and the region $\ell+1$. The region Ω_{L+1} surrounding the head corresponds to the ambient air which is considered unbounded and has negligible conductivity. Let μ be the magnetic permeability of Ω, supposed to be equal to that of the air. A model with three regions is common: the innermost region is the brain, the second one is the skull and the third one is the scalp. For a more accurate description of the head, other regions could be used, e.g., cerebrospinal fluid and/or distinct regions for gray and white matter.

For the sake of simplicity, let us consider the case of a single neural source, representable by a current dipole of moment $\mathbf{Q}$ located at $\boldsymbol{p}'$.

The source current density is given by

$$\mathbf{J}_s(\boldsymbol{p}) = \mathbf{Q}\delta(\boldsymbol{p} - \boldsymbol{p}'), \tag{2.12}$$

where $\delta(\boldsymbol{p} - \boldsymbol{p}')$ is the value at $\boldsymbol{p}$ of the Dirac delta function centered at $\boldsymbol{p}'$. Since the media are supposed to be linear, what follows can be easily extended to the general case of many dipoles by applying the superposition principle.

With the assumptions we made, the EEG forward problem can be formulated as

the following set of boundary value problems coupled by interface conditions:

$$\begin{cases} \sigma_\ell(\boldsymbol{p})\nabla^2\phi_\ell(\boldsymbol{p}) = S_\ell(\boldsymbol{p}), & \boldsymbol{p} \in \Omega_\ell, \\ \phi_\ell(\boldsymbol{p}) = \phi_{\ell+1}(\boldsymbol{p}), & \boldsymbol{p} \in \mathcal{I}_{\ell,\ell+1}|_{\ell \neq L}, \quad \ell = 1, \ldots, L, \\ \sigma_\ell \boldsymbol{n}(\boldsymbol{p}) \cdot \nabla\phi_\ell(\boldsymbol{p}) = \sigma_{\ell+1}\boldsymbol{n}(\boldsymbol{p}) \cdot \nabla\phi_{\ell+1}(\boldsymbol{p}), & \boldsymbol{p} \in \mathcal{I}_{\ell,\ell+1}, \end{cases} \tag{2.13}$$

where $\boldsymbol{n}(\boldsymbol{p})$ denotes the outward unit normal vector to the interface $\mathcal{I}_{\ell,\ell+1}$ at $\boldsymbol{p}$ and the source term $S_\ell(\boldsymbol{p})$ can be expressed as follows:

$$S_\ell(\boldsymbol{p}) = \begin{cases} \nabla \cdot (\mathbf{Q}\delta(\boldsymbol{p} - \boldsymbol{p}')), & \text{neural source at } \boldsymbol{p}' \in \Omega_\ell, \\ 0, & \text{otherwise.} \end{cases} \tag{2.14}$$

In particular, considering a certain region, it is clear that the governing PDE is a Poisson equation if a neural source is located in that region or a Laplace equation otherwise.

2.4. The MEG forward problem. The solution of the MEG forward problem involves the solution of a potential problem on the interfaces. As a matter of fact, an application of the curl operator to both sides of Equation (2.5), taking into account Equation (2.2c) and Equation (2.7), yields

$$\nabla^2\mathbf{B}(\boldsymbol{p}) = -\mu\nabla \times \mathbf{J}(\boldsymbol{p}), \tag{2.15}$$

where the current density on the right-hand side is given by Equation (2.10) if the potential at $\boldsymbol{p}$ is known.

With some vector calculus, it can be shown that the solution of Equation (2.15) under the assumption of a null magnetic field at an infinite distance from the sources, is given by the well-known Biot-Savart law [4]:

$$\mathbf{B}(\boldsymbol{p}) = \frac{\mu}{4\pi}\int_\Omega \mathbf{J}(\boldsymbol{p}^*) \times \frac{\boldsymbol{p} - \boldsymbol{p}^*}{\|\boldsymbol{p} - \boldsymbol{p}^*\|^3}\mathrm{d}v. \tag{2.16}$$

where $\mathrm{d}v$ is the volume element for Ω. [GF] I think here $\boldsymbol{p}^*$ is a point in Ω and $\mathrm{d}v$ is the volume element for Ω. We should probably mention the latter. Further, I believe this is the same as the Biot-Savart law. If so, we might consider mentioning that name as well. [SG] Biot-Savart and Ampere-Laplace are both used. However, in [4] the former is used, so it is better to follow the same way.

By using Equation (2.10), the integral above can be split into two parts, one $\mathbf{B}_s(\boldsymbol{p})$ relating to the contribution of the source current density and the other describing the contribution of volume current density:

$$\mathbf{B}(\boldsymbol{p}) = \mathbf{B}_s(\boldsymbol{p}) + \frac{\mu}{4\pi}\int_\Omega \sigma(\boldsymbol{p}^*)\nabla\phi(\boldsymbol{p}^*) \times \frac{\boldsymbol{p} - \boldsymbol{p}^*}{\|\boldsymbol{p} - \boldsymbol{p}^*\|^3}\mathrm{d}v, \tag{2.17}$$

where, for the considered dipole source, the first term is given by

$$\mathbf{B}_s(\boldsymbol{p}) = \frac{\mu}{4\pi}\mathbf{Q} \times \frac{\boldsymbol{p} - \boldsymbol{p}'}{\|\boldsymbol{p} - \boldsymbol{p}'\|^3}. \tag{2.18}$$

The volume integral over Ω in Equation (2.17) can be transformed into a surface integral over the interfaces. In fact, by applying the following corollary of the Divergence Theorem:

$$\int_\Omega \nabla \times \mathbf{P}\mathrm{d}v = \int_{\partial\Omega} \boldsymbol{n} \times \mathbf{P}\mathrm{d}s$$

with $\mathbf{P} = \frac{\boldsymbol{p}-\boldsymbol{p}^*}{\|\boldsymbol{p}-\boldsymbol{p}^*\|^3}$ and $\mathrm{d}v$ the surface element for $\partial\Omega$, and by remembering our nested compartment model of the brain, we obtain [3]

$$\mathbf{B}(\boldsymbol{p}) = \mathbf{B}_s(\boldsymbol{p}) + \frac{\mu}{4\pi}\sum_{\ell=1}^{L}(\sigma_{\ell+1}-\sigma_\ell)\int_{\mathcal{I}_{\ell,\ell+1}}\phi(\boldsymbol{p}^*)\boldsymbol{n}(\boldsymbol{p}^*)\times\frac{\boldsymbol{p}-\boldsymbol{p}^*}{\|\boldsymbol{p}-\boldsymbol{p}^*\|^3}\mathrm{d}s. \tag{2.19}$$

In this paper we focus our attention on the solution of the EEG forward problem which is the crucial step also in solving the MEG forward problem.

3. Methodology. Kernel-based methods are popular in many fields [30] because they allow for a meshfree solution to interpolation and BVPs with the potential for spectral accuracy. Among them, the Method of Fundamental Solutions (MFS) is a boundary-type method which has been successfully used to solve homogeneous elliptic PDEs [19]. It was first proposed by Kupradze and Aleksidze [31–33] for solving BVPs of the form:

$$\begin{cases}\mathcal{L}u(\boldsymbol{p}) = 0, & \boldsymbol{p}\in\Omega\subset\mathbb{R}^3,\\ \mathcal{T}u(\boldsymbol{p}) = f^{\partial\Omega}(\boldsymbol{p}), & \boldsymbol{p}\in\partial\Omega,\end{cases} \tag{3.1}$$

where $\mathcal{L}$ is the elliptic differential operator, $\partial\Omega$ is the boundary of the domain Ω, and $\mathcal{T}$ and $f^{\partial\Omega}$ are the operator and the known function defining the boundary conditions, respectively.
Like BEM, MFS is applicable when a *fundamental solution* of the PDE is known, i.e., a function $K : (\boldsymbol{p},\boldsymbol{q}) \mapsto K(\boldsymbol{p},\boldsymbol{q})$ such that

$$\mathcal{L}K(\boldsymbol{p},\boldsymbol{q}) = -\delta(\boldsymbol{p}-\boldsymbol{q}), \quad \boldsymbol{p},\boldsymbol{q}\in\mathbb{R}^3, \tag{3.2}$$

where K is defined everywhere except at $\boldsymbol{p} = \boldsymbol{q}$ giving rise to a *singularity* of the fundamental solution along this line.

3.1. The Method of Fundamental Solutions. The main idea of the MFS is to estimate the solution of the BVP (3.1) by means of a linear combination of fundamental solutions of the governing PDE, i.e.,

$$\hat{u}(\boldsymbol{p}) = \sum_{\xi_j\in\Xi} c_j K(\boldsymbol{p},\boldsymbol{\xi}_j), \quad \boldsymbol{p}\in\Omega, \tag{3.3}$$

where Ξ is a set of *centers* placed on a *fictitious boundary* outside the outside the physical domain in order to avoid the singularities of K in the representation of the solution. [SG] INSERT IMAGE FICTITIOUS BOUNDARIES
The coefficients c_j have to be determined by imposing upon (3.3) that it satisfy the boundary conditions at a set P of *collocation points*:

$$\sum_{\xi_j\in\Xi} c_j\mathcal{T}K(\boldsymbol{p}_i,\boldsymbol{\xi}_j) = f^{\partial\Omega}(\boldsymbol{p}_i) \quad \boldsymbol{p}_i\in P. \tag{3.4}$$

It is worth noting that only the satisfaction of the boundary conditions is required, thus reducing the dimension of the problem by one. Moreover, if a maximum principle holds, the following bound is satisfied:

$$\|u-\hat{u}\|_{\infty,\Omega} \le \|f^{\partial\Omega}-\mathcal{T}\hat{u}\|_{\infty,\partial\Omega}, \tag{3.5}$$

and therefore the overall approximation error is governed by the quality of the approximation of the right-hand side function $f^{\partial\Omega}$ by linear combinations of kernels of the form $\mathcal{T}K$ on the boundary alone.

3.2. Dealing with the fictitious boundary. MFS has other remarkable advantages. Above all, in general, neither special assumptions on the placement of collocation points and centers nor connectivity information are needed: pairwise distances between points, and normals to boundaries for certain problems, are the only geometric quantities involved, so this method is "truly meshfree". No numerical integration is required either, with remarkable savings in terms of computational cost with respect to mesh-based solvers and possibly avoiding difficulties in handling singular integrands involved in BEM formulations. Moreover, for certain problems and for smooth data and domains, this method was found to be spectrally convergent [23–25]. Further benefits come from the ease of implementation which makes computer codes very flexible. [GF] We've said this before, but perhaps it's good to repeat this summary. [SG] Actually I did say this again just to underline the pros of the method.

A key step in applying the MFS consists in locating the fictitious boundaries. Some authors claim that locating the fictitious boundaries is a controversial aspect of the MFS. This is certainly true in the sense that the position of the centers does affect the accuracy. In particular, the condition number depends on the distance of the centers relative to the boundary collocation points, so that the set of linear equations arising from boundary collocation can become highly ill-conditioned [34]. Actually, ill-conditioning is a common and discussed drawback of kernel-based methods [30,35,36].

Therefore particular care is needed in order to avoid inaccurate results. This observation motivated others formulations of the MFS. For example, Young *et al.* [37] and Chen *et al.* [38] proposed the Regularized Meshless Method (RMM) which remedies the singularities of the fundamental solution by employing a regularization technique based on subtracting and then adding-back certain terms. However, Song and Chen [39] showed that the RMM fails to provide a satisfactory accuracy for problems in arbitrary domains and even for problems in regular domains but with nonuniform distributions of collocation points. To remedy this drawback, they proposed an alternative approach but it requires numerical integration. Nevertheless, these approaches have been proposed for 2D problems only. [GF] I don't see the limitation to uniformly spaced nodes – at least not in [37]. However, it seems that this technique may not generalize so easily to 3D since one needs to be working with the "correct" kernel, i.e., a kernel which can be regularized by the techniques they use. As far as I can tell, they do only 2D fundamental solutions. I think I've see some similar work in the context of a 2D Stokes problem with BEM (a Ph.D. thesis at IIT some years back by Xu Sun). If I remember correctly he was extremely proud to have found something that worked for his problem by referring to earlier work by Kress, and I think 3D was considered to be out of reach. My point is, this may be very tricky business (and I don't understand it well enough). [SG] OK, a reference were missing there. Now it should sound a bit better.

Inspired by the RMM, Chen [40] proposed the Singular Boundary Method (SBM), which collocates centers in coincidence with collocation points on the physical boundaries by eliminating the singularity of the fundamental solutions via a numerical regularization technique referred to as "inverse interpolation technique". However this method is remarkably more costly than the MFS because it requires the solution of an additional linear system whose dimensions increase as the number of centers increases.

In order to achieve low computational costs, e.g., when forward solvers are intended to be inserted into an inverse framework, the classical MFS formulation is still attractive and the task of locating the fictitious boundaries can be accomplished by means of two different approaches, namely the *static* method and the *dynamic* one [20]. In the dynamic approach, the fictitious boundaries are determined together

with the solution by a time-consuming procedure which involves nonlinear optimization routines.

In the static approach, the locations of centers are pre-assigned. The theoretical basis of the static method is provided in [23, 41] for centers uniformly distributed on circles (2D) or spheres (3D). Best results are theoretically provided with the radius of the circle or the sphere approaching infinity; however the resulting system is increasingly affected by ill-conditioning as centers move towards infinity, therefore a compromise has to be reached.

A more natural choice is to take fictitious boundaries via an inflation/deflation procedure of the physical boundaries [SG] REFERENCE TO IMAGE. In [42] it is demonstrated by numerical experiments that this setting is superior to the one in which fictitious boundaries are taken to be circles or a spheres. Our experiments have shown that a static approach coupled with inflation/deflation is reliable, easy to implement and computationally inexpensive. Moreover, standard regularization techniques usually help to overcome stability problems, in spite of the actual value of the condition number [35].

3.3. The Method of Particular Solutions. So far we have discussed solutions of homogeneous BVPs. However, MFS can be also applied for solving inhomogeneous BVPs via an application of the Method of Particular Solutions (MPS) [19].

Let us consider an inhomogeneous BVP of the form

$$\begin{cases} \mathcal{L}u(\boldsymbol{p}) = f^{\Omega}(\boldsymbol{p}), & \boldsymbol{p} \in \Omega \subseteq \mathbb{R}^3, \\ \mathcal{T}u(\boldsymbol{p}) = f^{\partial\Omega}(\boldsymbol{p}), & \boldsymbol{p} \in \partial\Omega. \end{cases} \tag{3.6}$$

We call a *particular solution* of the BVP (3.6) a function defined on $\Omega \cup \partial\Omega$ which satisfies the PDE but not necessarily the boundary conditions.

The problem (3.6) can be reduced to a homogeneous one by considering u as the sum of a particular solution u_p and its associated homogeneous solution u_h, i.e.,

$$u = u_h + u_p. \tag{3.7}$$

Then we get the following homogeneous BVP for u_h:

$$\begin{cases} \mathcal{L}u_h(\boldsymbol{p}) = f^{\Omega}(\boldsymbol{p}) - \mathcal{L}u_p(\boldsymbol{p}) = 0, & \boldsymbol{p} \in \Omega, \\ \mathcal{T}u_h(\boldsymbol{p}) = f^{\partial\Omega}(\boldsymbol{p}) - \mathcal{T}u_p(\boldsymbol{p}), & \boldsymbol{p} \in \partial\Omega. \end{cases} \tag{3.8}$$

Therefore, if u_p is known, u can be estimated by approximating the term u_h via MFS. Actually, the same procedure has been proposed for solving the M/EEG forward problem both in the FEM [8, 43] and in the meshfree [17, 18] literature where it is referred to as the "subtraction method" or "singularity separation method".

3.4. MFS/MPS applied to coupled BVPs. We have shown that, for a piecewise-constant conductivity head model, the EEG forward problem can be formulated as the set of coupled BVPs (2.13). The governing PDE in the region ℓ may be homogeneous or inhomogeneous depending on the absence or the presence, respectively, of a neural source in the region. While MFS can be applied directly in the former case, in the latter case the solution has to be sought via MPS. For the sake of generality, let us introduce a parameter α_ℓ such that

$$\alpha_\ell = \begin{cases} 1, & \text{if the source is in } \Omega_\ell, \\ 0, & \text{otherwise.} \end{cases} \tag{3.9}$$

This enables us to express the potential function in the ℓ-th region as

$$\phi_\ell(\boldsymbol{p}) = \phi_{h,\ell}(\boldsymbol{p}) + \alpha_\ell \phi_{p,\ell}(\boldsymbol{p}). \tag{3.10}$$

On the one hand, an analytical expression for a function that satisfies the equation

$$\sigma_\ell \nabla^2 \phi(\boldsymbol{p}) = \nabla \cdot (\mathbf{Q}\delta(\boldsymbol{p} - \boldsymbol{p}')) \tag{3.11}$$

in an unbounded domain, is known [4]:

$$\phi_{p,\ell}(\boldsymbol{p}) = \frac{1}{4\pi\sigma_\ell} \frac{\boldsymbol{p} - \boldsymbol{p}'}{\|\boldsymbol{p} - \boldsymbol{p}'\|^3} \cdot \mathbf{Q}. \tag{3.12}$$

This function is clearly a particular solution of the governing PDE of the BVP when a neural source is located at $\boldsymbol{p}' \in \Omega_\ell$.
On the other hand, $\phi_{h,\ell}$ is given by the solution of the following BVP:

$$\begin{cases} \nabla^2 \phi_{h,\ell}(\boldsymbol{p}) = 0, & \boldsymbol{p} \in \Omega_\ell, \\ \phi_{h,\ell}(\boldsymbol{p}) - \phi_{h,\ell+1}(\boldsymbol{p}) = \alpha_{\ell+1}\phi_{p,\ell+1}(\boldsymbol{p}) - \alpha_\ell \phi_{p,\ell}(\boldsymbol{p}), & \boldsymbol{p} \in \mathcal{I}_{\ell,\ell+1}|_{\ell \neq L}, \\ \sigma_\ell \boldsymbol{n}(\boldsymbol{p}) \cdot \nabla \phi_{h,\ell}(\boldsymbol{p}) - \sigma_{\ell+1} \boldsymbol{n}(\boldsymbol{p}) \cdot \nabla \phi_{h,\ell+1}(\boldsymbol{p}) = & \\ = \alpha_{\ell+1}\sigma_{\ell+1} \boldsymbol{n}(\boldsymbol{p}) \cdot \nabla \phi_{p,\ell+1}(\boldsymbol{p}) - \alpha_\ell \sigma_\ell \boldsymbol{n}(\boldsymbol{p}) \cdot \nabla \phi_{p,\ell}(\boldsymbol{p}) & \boldsymbol{p} \in \mathcal{I}_{\ell,\ell+1}. \end{cases} \tag{3.13}$$

In this case, the homogeneous part of the potential can be approximated, by means of MFS, as a linear combination of fundamental solutions for the Laplace equation:

$$\hat{\phi}_{h,\ell}(\boldsymbol{p}) = \sum_{\xi_j \in \Xi_\ell} c_j^\ell K(\boldsymbol{p}, \boldsymbol{\xi}_j), \quad \boldsymbol{p} \in \Omega_\ell, \tag{3.14}$$

where Ξ_ℓ is the set of centers relative to the region Ω_ℓ and the fundamental solution for the Laplace equation in 3D is

$$K(\boldsymbol{p}, \boldsymbol{q}) = \frac{1}{4\pi\|\boldsymbol{p} - \boldsymbol{q}\|}. \tag{3.15}$$

In order to determine the L sets of coefficients $\{\boldsymbol{c}^\ell\}_{\ell=1}^L$, the collocation has to be performed on each interface. To this end, let $P^{\mathcal{D}}_{\ell,\ell+1}$ and $P^{\mathcal{N}}_{\ell,\ell+1}$ be the sets of collocation points on the interface $\mathcal{I}_{\ell,\ell+1}$ where we, respectively, impose Dirichlet and Neumann conditions.

Then collocation yields the following coupled linear system:

$$\mathsf{A}\boldsymbol{c} = \boldsymbol{b}, \tag{3.16}$$

where

$$\mathsf{A} = \begin{bmatrix} \mathsf{D}^1_{1,2} & \mathsf{D}^2_{1,2} & & & & & & & & \\ \mathsf{N}^1_{1,2} & \mathsf{N}^2_{1,2} & & & & & & & & \\ & \mathsf{D}^2_{2,3} & \mathsf{D}^3_{2,3} & & & & & & & \\ & \mathsf{N}^2_{2,3} & \mathsf{N}^3_{2,3} & & & & & & & \\ & & & \ddots & & & & & & \\ & & & & \mathsf{D}^\ell_{\ell,\ell+1} & \mathsf{D}^{\ell+1}_{\ell,\ell+1} & & & & \\ & & & & \mathsf{N}^\ell_{\ell,\ell+1} & \mathsf{N}^{\ell+1}_{\ell,\ell+1} & & & & \\ & & & & & & \ddots & & & \\ & & & & & & & \mathsf{D}^{L-1}_{L-1,L} & \mathsf{D}^L_{L-1,L} \\ & & & & & & & \mathsf{N}^{L-1}_{L-1,L} & \mathsf{N}^L_{L-1,L} \\ & & & & & & & & \mathsf{N}^L_{L,L+1} \end{bmatrix};$$

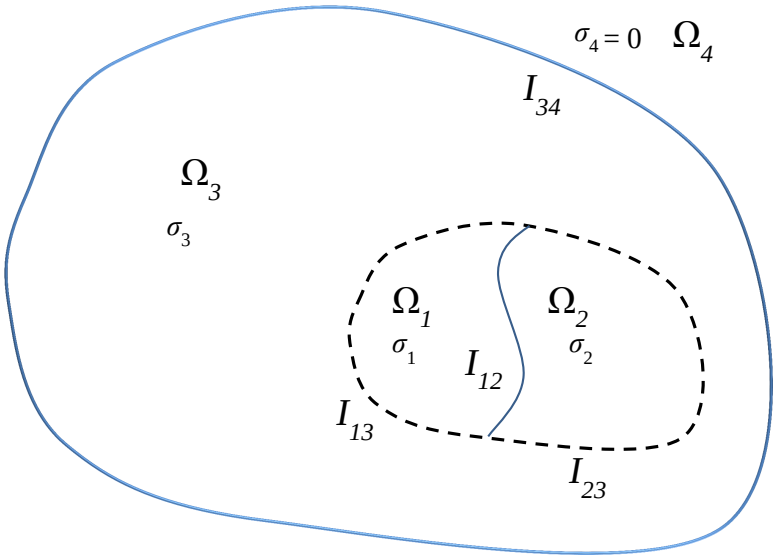

FIG. 3.1. *Example of head model with non-nested regions. EDIT this figure (work in progress)*

$$\boldsymbol{c} = \begin{bmatrix} \boldsymbol{c}^1 & \boldsymbol{c}^2 & \cdots & \boldsymbol{c}^\ell & \cdots & \boldsymbol{c}^{L-1} & \boldsymbol{c}^L \end{bmatrix}^{\mathrm{T}};$$

$$\boldsymbol{b} = \begin{bmatrix} \boldsymbol{b}^{\mathcal{D}}_{1,2} & \boldsymbol{b}^{\mathcal{N}}_{1,2} & \boldsymbol{b}^{\mathcal{D}}_{2,3} & \boldsymbol{b}^{\mathcal{N}}_{2,3} & \cdots & \boldsymbol{b}^{\mathcal{D}}_{\ell,\ell+1} & \boldsymbol{b}^{\mathcal{N}}_{\ell,\ell+1} & \cdots & \boldsymbol{b}^{\mathcal{D}}_{L-1,L} & \boldsymbol{b}^{\mathcal{N}}_{L-1,L} & \boldsymbol{b}^{\mathcal{N}}_{L,L+1} \end{bmatrix}^{\mathrm{T}}$$

with

$$\begin{aligned}
(\mathsf{D}^{\ell}_{\ell,\ell+1})_{ij} &= K(\boldsymbol{p}_i, \boldsymbol{\xi}_j) && \boldsymbol{p}_i \in P^{\mathcal{D}}_{\ell,\ell+1}, \quad \boldsymbol{\xi}_j \in \Xi_\ell, \\
(\mathsf{D}^{\ell+1}_{\ell,\ell+1})_{ij} &= -K(\boldsymbol{p}_i, \boldsymbol{\xi}_j) && \boldsymbol{p}_i \in P^{\mathcal{D}}_{\ell,\ell+1}, \quad \boldsymbol{\xi}_j \in \Xi_{\ell+1}, \\
(\mathsf{N}^{\ell}_{\ell,\ell+1})_{ij} &= \sigma_\ell \boldsymbol{n}(\boldsymbol{p}_i) \cdot \nabla K(\boldsymbol{p}_i, \boldsymbol{\xi}_j) && \boldsymbol{p}_i \in P^{\mathcal{N}}_{\ell,\ell+1}, \quad \boldsymbol{\xi}_j \in \Xi_\ell, \\
(\mathsf{N}^{\ell+1}_{\ell,\ell+1})_{ij} &= -\sigma_{\ell+1} \boldsymbol{n}(\boldsymbol{p}_i) \cdot \nabla K(\boldsymbol{p}_i, \boldsymbol{\xi}_j) && \boldsymbol{p}_i \in P^{\mathcal{N}}_{\ell,\ell+1}, \quad \boldsymbol{\xi}_j \in \Xi_{\ell+1}, \\
(\boldsymbol{b}^{\mathcal{D}}_{\ell,\ell+1})_i &= \alpha_{\ell+1}\phi_{p,\ell+1}(\boldsymbol{p}_i) - \alpha_\ell \phi_{p,\ell}(\boldsymbol{p}_i) && \boldsymbol{p}_i \in P^{\mathcal{D}}_{\ell,\ell+1}, \\
(\boldsymbol{b}^{\mathcal{N}}_{\ell,\ell+1})_i &= \alpha_{\ell+1}\sigma_{\ell+1}\boldsymbol{n}(\boldsymbol{p}_i) \cdot \nabla \phi_{p,\ell+1}(\boldsymbol{p}_i) - \alpha_\ell \sigma_\ell \boldsymbol{n}(\boldsymbol{p}_i) \cdot \nabla \phi_{p,\ell}(\boldsymbol{p}_i) && \boldsymbol{p}_i \in P^{\mathcal{N}}_{\ell,\ell+1}.
\end{aligned}$$

3.5. Head models with non-nested compartments. Nested models are not able to represent brain and skull defects due to surgery or pathological conditions, whose effect on localization accuracy may be significant [44]. It is worth noting that the formulation presented above can be straightforwardly generalized to a domain with non-nested compartments. Such a setting can be potentially useful to obtain more realistic head models.

Here, as an example, the linear system arising from a domain with non-nested

regions shown in Figure 3.1 is reported:

$$\begin{bmatrix} \mathsf{D}^1_{1,2} & \mathsf{D}^2_{1,2} & & \\ \mathsf{N}^1_{1,2} & \mathsf{N}^2_{1,2} & & \\ \mathsf{D}^1_{1,3} & & \mathsf{D}^3_{1,3} & \\ \mathsf{N}^1_{1,3} & & \mathsf{N}^3_{1,3} & \\ & \mathsf{D}^2_{2,3} & \mathsf{D}^3_{2,3} & \\ & \mathsf{N}^2_{2,3} & \mathsf{N}^3_{2,3} & \\ & & \mathsf{N}^3_{3,4} & \end{bmatrix} \begin{bmatrix} \boldsymbol{c}^1 \\ \boldsymbol{c}^2 \\ \boldsymbol{c}^3 \end{bmatrix} = \begin{bmatrix} \boldsymbol{b}^{\mathcal{D}}_{1,2} \\ \boldsymbol{b}^{\mathcal{N}}_{1,2} \\ \boldsymbol{b}^{\mathcal{D}}_{1,3} \\ \boldsymbol{b}^{\mathcal{N}}_{1,3} \\ \boldsymbol{b}^{\mathcal{D}}_{2,3} \\ \boldsymbol{b}^{\mathcal{N}}_{2,3} \\ \boldsymbol{b}^{\mathcal{N}}_{3,4} \end{bmatrix}.$$

4. Numerical Results. In order to validate the proposed approach, numerical experiments have been carried out concerning the potential problem (EEG) for simple spherical head geometries for which analytical or semi-analytical solutions are known. The MFS is compared with a state-of-the-art BEM formulation implemented in a popular toolbox for M/EEG analysis [15]. A variety of versions of MFS solvers are tested, namely with different ratios R_{MFS} between number of centers and number of collocation points, i.e., the linear system in Equation (3.16) is overdetermined and solved in the least squares sense.

Collocation points are nearly uniformly distributed over spherical boundaries by means of golden section spirals. However, experiments not reported here have shown that a random distribution of boundary collocation points does not affect accuracy significantly.

Centers are located by a procedure of inflation/deflation of physical surfaces, thus they are distributed starting from the set of collocation points by random reduction. Convergence tests have been conducted and CPU times and condition numbers of the system matrix have been recorded. The numerical experiments have been conducted on a Lenovo TS D30 equipped with a six core Intel Xeon E5-2630 @ 2.30GHz and 24GB of RAM. All the surface potentials have been referred to the potential at a point arbitrarily chosen as a reference. The accuracy is measured by means of the 2-norm relative error.

The MFS linear system has been solved by the Singular Values Decomposition (SVD). Tests not reported here have shown that least-squares solutions present the same accuracy. [GF] If this is really true, then why spend the extra effort that goes into using the SVD? I would ask this if I were the referee. [SG] Instead of reporting a comparison between SVD and TRM (Table 4.2) we can report the comparison between LSM and TRM and say that a significant improvement in accuracy, when R_{MFS} is high (0.8), can be obtained by TRM at an extra computational cost. In Figure 4.3 we can show only the better results in terms of accuracy, by specifying the used methods in the legend. Do you think that it would sound good? The Tikhonov regularization method (TRM) with an L-curve corner criterion for the determination of the regularization parameter [45] has also been adopted in order to improve the solution for certain case studies.

4.1. A homogeneous-sphere head model. A first set of simulations has been performed by considering a homogeneous-sphere head model. Such a model is usually not adequate for practical purposes and no coupling is involved, but an analytical solution is known for the EEG forward problem [46]. A unitary current dipole of moment $(1, 0, 0)$ A·m was located at $(0, 0, 0.06)$ m in a homogeneous sphere of radius 0.1 m and conductivity 0.2 S/m.

For this setting, Figure 4.1(a) shows the convergence plot both for BEM and MFS solvers. Regardless of the ratio R_{MFS}, the MFS clearly outperforms BEM. MFS

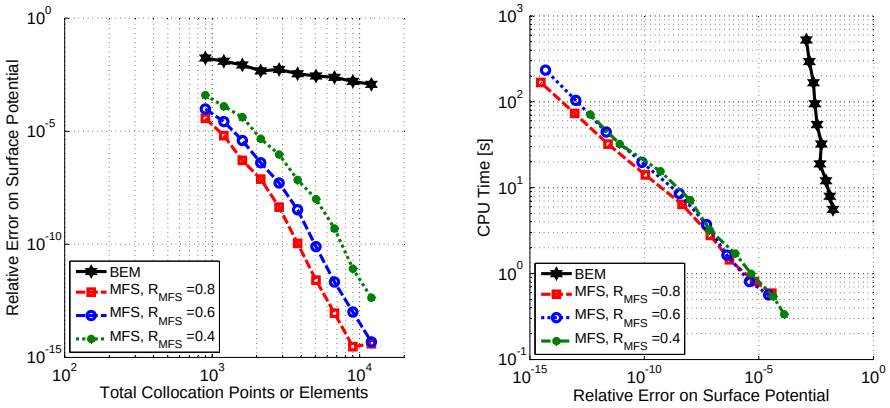

(a) Convergence (b) Cost per Accuracy

FIG. 4.1. *Dipole in a homogeneous sphere.*

shows exponential convergence while BEM convergence is algebraic. In particular, the convergence rate increases with R_{MFS}.
A cost per accuracy plot is reported in Figure 4.1(b). This plot is useful in relating the computational effort and the accuracy in light of the application of the forward solver in the inverse framework. For this problem, the proposed approach is clearly superior to BEM.
In all cases, the linear systems turn out not to be affected by ill-conditioning as demonstrated by the values reported in Table 4.1.

TABLE 4.1
Condition number for MFS systems arising in the homogeneous sphere model case.

N	Condition number		
	$R_{MFS} = 0.8$	$R_{MFS} = 0.6$	$R_{MFS} = 0.4$
898	2.5692e+04	5.8219e+03	9.4517e+02
1198	9.0743e+04	1.9052e+04	2.9867e+03
1600	5.4927e+05	6.6192e+04	9.8789e+03
2132	1.9179e+06	2.9571e+05	3.5692e+04
2844	1.2072e+07	1.5294e+06	1.4981e+05
3792	1.0463e+08	9.7741e+06	7.1930e+05
5058	1.0820e+09	7.8999e+07	4.2044e+06
6744	1.6401e+10	9.3290e+08	3.1941e+07
8994	4.3950e+11	1.4783e+10	3.1937e+08
11994	1.5840e+13	3.5971e+11	4.5002e+09

For the homogeneous sphere case study, Figure 4.2 reports analytic and computed potential distributions and error distributions on the sphere, corresponding to BEM and MFS ($R_{MFS} = 0.8$) computation with nearly 12000 elements or collocation points. [GF] Is there something missing in the BEM error plot? It seems to be saying that the BEM error is on the order of 1, while MFS is 10^{-11}. Shouldn't BEM be something like 10^{-3} or so? [SG] As you say in the note about the next plot, we have the absolute error here. Do you think that this difference may be confusing?

4.2. A multi-layered sphere head model. Similar experiments have been conducted for a dipole of moment $(1, 0, 0)$ A·m located at $(0, 0, 0.0522)$ m in the innermost layer of a three-layered sphere with radii 0.087 m, 0.092 m and 0.1 m and conductivities 0.33 S/m, 0.0125 S/m, 0.33 S/m, respectively. It is worth noting that, though the geometrical shape is still simplistic for such a model, both the physical properties and the geometrical sizes closely approximate the realistic ones. Moreover, a semi-analytical expression of the electric potential on the outermost sphere is known [47, 48].

Table 4.2 shows a comparison among MFS solvers by adopting SVD and TRM. Our tests show that the solution is sensitive to Tikhonov regularization by increasing the R_{MFS} ratio and/or the number of collocation points. (This behavior seems to be related to the observation that regularization has no effect when too few data are available.)

TABLE 4.2
Relative error comparison among MFS solvers for three-layered sphere model with Singular Values Decomposition (SVD) and Tikhonov regularization method (TRM).

N	Relative Error					
	$R_{MFS} = 0.8$		$R_{MFS} = 0.6$		$R_{MFS} = 0.4$	
	SVD	TRM	SVD	TRM	SVD	TRM
900	2.0787e-02	3.1837e-02	8.4967e-02	1.4094e-01	2.3292e-01	2.7871e-01
1200	1.0011e-02	8.2940e-03	3.0714e-02	6.5069e-02	1.1863e-01	1.6618e-01
1598	1.2686e-02	7.4075e-03	1.3294e-02	1.7079e-02	4.1477e-02	6.3405e-02
2134	2.3447e-02	4.7605e-03	5.9253e-03	6.8213e-03	2.1018e-02	2.4387e-02
2842	3.4490e-02	1.6720e-03	4.3129e-03	2.1690e-03	1.0102e-02	1.0913e-02
3794	2.1767e-03	2.3381e-04	2.7617e-03	9.2186e-04	5.0114e-03	6.5334e-03
5058	3.8408e-04	4.7749e-05	1.9991e-04	7.4911e-05	1.3819e-03	1.8530e-03
6744	1.1143e-05	9.6754e-06	1.7674e-05	1.2020e-05	2.7331e-04	3.2012e-04
8994	7.3112e-07	4.8529e-07	4.1609e-06	2.5859e-06	4.7753e-05	4.1486e-05
11996	1.3538e-07	4.1344e-08	2.7093e-07	2.0503e-07	1.2362e-05	8.7958e-06

In all cases, the linear systems turn out not to be affected by ill-conditioning as demonstrated by the values reported in Table 4.3.

TABLE 4.3
Condition number for MFS systems arising in the three-layered sphere model case.

N	Condition number		
	$R_{MFS} = 0.8$	$R_{MFS} = 0.6$	$R_{MFS} = 0.4$
900	4.9069e+04	1.5725e+04	5.2497e+03
1200	1.1081e+05	3.5029e+04	1.0500e+04
1598	3.5211e+05	8.5067e+04	2.1998e+04
2134	3.3080e+06	2.7242e+05	4.8752e+04
2842	1.4921e+07	1.6631e+06	1.1858e+05
3794	7.4951e+07	7.1127e+06	4.5564e+05
5058	2.5300e+08	4.7812e+07	1.1088e+06
6744	1.0490e+09	1.6835e+08	5.3191e+06
8994	2.0654e+10	9.9322e+08	6.0796e+07
11996	8.2855e+12	2.0662e+10	4.1392e+08

The convergence behavior is reported in Figure 4.3(a), where MFS solutions are obtained by TRM. Also in this case, spectral convergence is observed, with a rate that is directly related to R_{MFS}.
The cost per accuracy plot is reported in Figure 4.3(b). For this more realistic head model, the MFS is again extremely competitive when compared to BEM. However, from an accuracy vs. CPU time standpoint, the advantage becomes more significant as the desired accuracy increases.

For the three-layered sphere case study, Figure 4.4 reports analytic and computed potential distributions and error distributions on the sphere corresponding to BEM and MFS ($R_{MFS} = 0.8$) computation with nearly 12000 elements or collocation points. [GF] Similar remark about the plots as before. Shouldn't BEM here be around 10^{-2}? Or is this because the convergence plots report relative errors, and the surface plots have absolute error?

5. Conclusions. Both the EEG and MEG forward problems for a piecewise-constant conductivity head model can be formulated as a set of coupled BVPs. In this paper we have shown that the solution can be sought by the Method of Fundamental Solutions (MFS) via the Method of Particular Solutions (MPS). The proposed method is a boundary-type, integration-free and easy-to-implement alternative to mesh-based methods. The method is truly meshfree, therefore no meshing algorithms have to be run in a pre-processing stage in order to discretize the head. On the one hand, this makes experiment setup easier and less expensive in terms of time. On the other hand, possible mesh-related artifacts in the solution are avoided.
We have compared the proposed method with the state-of-the-art implementation of the commonly used Boundary Element Method (BEM) in solving the EEG forward problem with spherical head models, for which analytical or semi-analytical solutions are known. A clear superiority of the MFS emerged from the comparison. From an accuracy standpoint, [GF] I'm pretty confident in our method, but I don't know if I want to go as far as putting it in (this strong) writing – also in the abstract. Do we have reason to be this cocky? Are we convinced we'll do similarly well for real geometries, and for inverse problems. I hope we will, in part based on the convergence behavior we've observed... [SG] Are you referring to the spectral convergence, to the claimed "clear superiority" or both? The convergence plots seems to suggest exponential convergence. However, generally speaking, it might be better to maintain a low profile until we have a comparison in the inverse problem field. Thus, I'd remove the sentence on the "clear superiority". I'd also re-propose a concept we gave in Introduction, i.e., that our method runs faster than BEM without sacrificing accuracy. the proposed method shows spectral convergence while the BEM convergence is only algebraic. Moreover, from a cost per accuracy standpoint, the MFS allows for a saving in CPU time that is as savings in pre-processing stage we did not quantify because of the simplicity of the considered head geometries, the MFS allows for a saving in CPU time that becomes more significant as we demand higher accuracy. This advantage will play an important role when we apply the forward solver within the iterative solve of the inverse problem needed for the localization of the sources of neural activity. Moreover, further savings in terms of time come from the elimination of the meshing task from the pre-processing stage.

6. Acknowledgments. This work is partially supported by FFR2012 Project from University of Palermo. The research of the second author is partially supported by NSF Grant DMS–1115392.

REFERENCES

[1] P.L. Nunez. *Electric fields of the brain: the neurophysics of EEG*. Oxford University Press, 2006.

[2] E. Niedermeyer and F.L. da Silva. *Electroencephalography: Basic Principles, Clinical Applications, and Related Fields*. Lippincott Williams & Wilkins, 2012.

[3] M. Hämäläinen, R. Hari, R.J. Ilmoniemi, J. Knuutila, and O.V. Lounasmaa. Magnetoencephalography—theory, instrumentation, and applications to noninvasive studies of the working human brain. *Reviews of Modern Physics*, 65(2):413–497, 1993.

[4] J. Sarvas. Basic mathematical and electromagnetic concepts of the biomagnetic inverse problem. *Physics in Medicine and Biology*, 32(1):11, 1987.

[5] R. Grech, T. Cassar, J. Muscat, K. Camilleri, S. Fabri, M. Zervakis, P. Xanthopoulos, V. Sakkalis, and B. Vanrumste. Review on solving the inverse problem in EEG source analysis. *Journal of NeuroEngineering and Rehabilitation*, 5(25), 2008.

[6] L. Homa, D. Calvetti, A. Hoover, and E. Somersalo. Bayesian preconditioned CGLS for source separation in MEG time series. *SIAM Journal on Scientific Computing*, 35(3):B778–B798, 2013.

[7] Y. Yan, P. Nunez, and R. Hart. Finite-element model of the human head: scalp potentials due to dipole sources. *Medical and Biological Engineering and Computing*, 29(5):475–481, 1991.

[8] S.P. Broeh, H. Zhou, and M.J. Peters. Computation of neuromagnetic fields using finite-element method and Biot-Savart law. *Medical and Biological Engineering and Computing*, 34(1):21–26, 1996.

[9] C.H. Wolters, M. Kuhn, A. Anwander, and S. Reitzinger. A parallel algebraic multigrid solver for finite element method based source localization in the human brain. *Computing and Visualization in Science*, 5(3):165–177, 2002.

[10] B. He, T. Musha, Y. Okamoto, S. Homma, Y. Nakajima, and T. Sato. Electric dipole tracing in the brain by means of the boundary element method and its accuracy. *IEEE Transactions on Biomedical Engineering*, 34(6):406–414, 1987.

[11] M. Hämäläinen and J. Sarvas. Realistic conductivity geometry model of the human head for interpretation of neuromagnetic data. *IEEE Transactions on Biomedical Engineering*, 36(2):165–171, 1989.

[12] A. Zeynep and G. Gençer. An advanced boundary element method (BEM) implementation for the forward problem of electromagnetic source imaging. *Physics in Medicine and Biology*, 49(21):5011–5028, 2004.

[13] J. Kybic, M. Clerc, T. Abboud, O. Faugeras, R. Keriven, and T. Papadopoulo. A common formalism for the integral formulations of the forward EEG problem. *IEEE Transactions on Medical Imaging*, 24(1):12–28, 2005.

[14] H. Hallez, B. Vanrumste, R. Grech, J. Muscat, W. De Clercq, A. Vergult, Y. D'Asseler, K. Camilleri, S. Fabri, S. Van Huffel, and I. Lemahieu. Review on solving the forward problem in EEG source analysis. *Journal of NeuroEngineering and Rehabilitation*, 4(1), 2007.

[15] R. Oostenveld, P. Fries, E. Maris, and J.M. Schoffelen. FieldTrip: open source software for advanced analysis of MEG, EEG, and invasive electrophysiological data. *Computational intelligence and neuroscience*, 2011:1, 2011.

[16] F. Tadel, S. Baillet, J.C. Mosher, D. Pantazis, and R.M. Leahy. Brainstorm: a user-friendly application for MEG/EEG analysis. *Computational intelligence and neuroscience*, 2011:8, 2011.

[17] N. von Ellenrieder, C.H. Muravchik, and A. Nehorai. A meshless method for solving the EEG forward problem. *IEEE Transactions on Biomedical Engineering*, 52(2):249 –257, 2005.

[18] G. Ala, G. Di Blasi, and E. Francomano. A numerical meshless particle method in solving the magnetoencephalography forward problem. *International Journal of Numerical Modelling: Electronic Networks, Devices and Fields*, 25(5-6):428–440, 2012.

[19] G. Fairweather and A. Karageorghis. The method of fundamental solutions for elliptic boundary value problems. *Advances in Computational Mathematics*, 9(1):69–95, 1998.

[20] M.A. Golberg and C.S. Chen. *The method of fundamental solutions for potential, Helmholtz and diffusion problems*, pages 103–176. Computational Mechanics Publications, 1998.

[21] Y. Smyrlis and A. Karageorghis. The method of fundamental solutions for stationary heat conduction problems in rotationally symmetric domains. *SIAM Journal on Scientific Computing*, 27(4):1493–1512, 2006.

[22] C. Alves and P. Antunes. The method of fundamental solutions applied to some inverse eigenproblems. *SIAM Journal on Scientific Computing*, 35(3):A1689–A1708, 2013.

[23] R.S.C. Cheng. *Delta-trigonometric and spline methods using the singlelayer potential representation*. PhD thesis, University of Maryland, 1987.
[24] M. Katsurada. Charge simulation method using exterior mapping functions. *Japan journal of industrial and applied mathematics*, 11(1):47–61, 1994.
[25] M. Katsurada and H. Okamoto. The collocation points of the fundamental solution method for the potential problem. *Computers & Mathematics with Applications*, 31(1):123–137, 1996.
[26] Y. Okada. Neurogenesis of evoked magnetic fields. In S.H. Williamson, G.L. Romani, L. Kaufman, and I. Modena, editors, *Biomagnetism: an Interdisciplinary Approach*, pages 399–408. Plenum Press, New York, 1983.
[27] R. Plonsey. *Bioelectric phenomena*. Wiley Online Library, 1969.
[28] J.C. de Munck, B.W. van Dijk, and H. Spekreijse. Mathematical dipoles are adequate to describe realistic generators of human brain activity. *IEEE Transactions on Biomedical Engineering*, 35(11):960 –966, 1988.
[29] R. Plonsey and D. Heppner. Considerations of quasi-stationarity in electrophysiological systems. *Bulletin of Mathematical Biology*, 29(4):657–664, 1967.
[30] G. E. Fasshauer. *Meshfree Approximation Methods with* MATLAB. World Scientific Publishing Co., Inc., River Edge, NJ, USA, 2007.
[31] V.D. Kupradze and M.A. Aleksidze. A method for the approximate solution of limiting problems in mathematical physics. *U.S.S.R. Computational Mathematics and Mathematical Physics*, 4:199–205, 1964.
[32] V.D. Kupradze and M.A. Aleksidze. The method of functional equations for the approximate solution of certain boundary value problems. *U.S.S.R. Computational Mathematics and Mathematical Physics*, 4:82–126, 1964.
[33] V.D. Kupradze. On the approximate solution of problems in mathematical physics. *Russian Mathematical Surveys*, 22:58–108, 1967.
[34] C.S. Chen, H.A. Cho, and M.A. Golberg. Some comments on the ill-conditioning of the method of fundamental solutions. *Engineering Analysis with Boundary Elements*, 30(5):405–410, 2006.
[35] P. A. Ramachandran. Method of fundamental solutions: singular value decomposition analysis. *Communications in Numerical Methods in Engineering*, 18(11):789–801, 2002.
[36] G. Fasshauer and M. McCourt. Stable evaluation of Gaussian radial basis function interpolants. *SIAM Journal on Scientific Computing*, 34(2):A737–A762, 2012.
[37] D.L. Young, K.H. Chen, and C.W. Lee. Novel meshless method for solving the potential problems with arbitrary domain. *Journal of Computational Physics*, 209(1):290–321, 2005.
[38] K.H. Chen, J.H. Kao, J.T. Chen, D.L. Young, and M.C. Lu. Regularized meshless method for multiply-connected-domain Laplace problems. *Engineering Analysis with Boundary Elements*, 30(10):882–896, 2006.
[39] R. Song and W. Chen. An investigation on the regularized meshless method for irregular domain problems. *Computer Modeling in Engineering and Sciences (CMES)*, 42(1):59, 2009.
[40] W. Chen, Z. Fu, and X. Wei. Potential problems by singular boundary method satisfying moment condition. *Computer Modeling in Engineering and Sciences (CMES)*, 54(1):65, 2009.
[41] A. Bogomolny. Fundamental solutions method for elliptic boundary value problems. *SIAM Journal on Numerical Analysis*, 22(4):644–669, 1985.
[42] P. Gorzelańczyk and J.A. Kołodziej. Some remarks concerning the shape of the source contour with application of the method of fundamental solutions to elastic torsion of prismatic rods. *Engineering Analysis with Boundary Elements*, 32(1):64–75, 2008.
[43] C.H. Wolters, H. Köstler, C. Möller, J. Härdtlein, L. Grasedyck, and W. Hackbusch. Numerical mathematics of the subtraction method for the modeling of a current dipole in EEG source reconstruction using finite element head models. *SIAM Journal on Scientific Computing*, 30(1):24–45, 2008.
[44] C.G. Bénar and J. Gotman. Modeling of post-surgical brain and skull defects in the EEG inverse problem with the boundary element method. *Clinical Neurophysiology*, 113(1):48–56, 2002.
[45] P.C. Hansen and D.P. O'Leary. The use of the L-curve in the regularization of discrete ill-posed problems. *SIAM Journal on Scientific Computing*, 14(6):1487–1503, 1993.
[46] D. Yao. Electric potential produced by a dipole in a homogeneous conducting sphere. *IEEE Transactions on Biomedical Engineering*, 47(7):964–966, 2000.
[47] J.C. de Munck and M.J. Peters. A fast method to compute the potential in the multisphere model. *IEEE Transactions on Biomedical Engineering*, 40(11):1166–1174, 1993.
[48] Z. Zhang. A fast method to compute surface potentials generated by dipoles within multilayer anisotropic spheres. *Physics in Medicine and Biology*, 40(3):335, 1995.

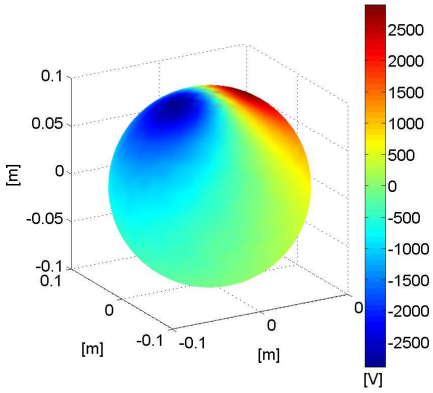

(a) Analytic surface potential

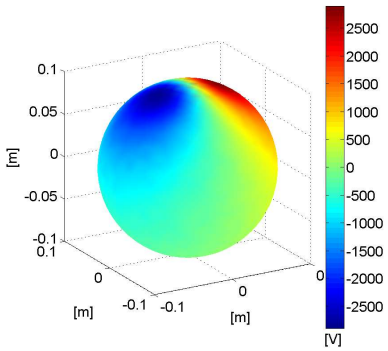

(b) BEM computed potential

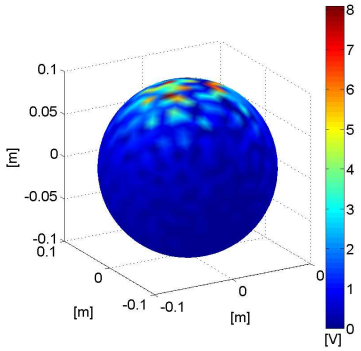

(c) BEM absolute error

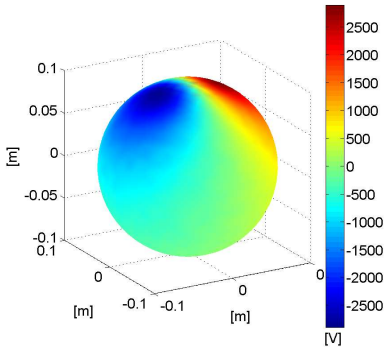

(d) MFS computed potential

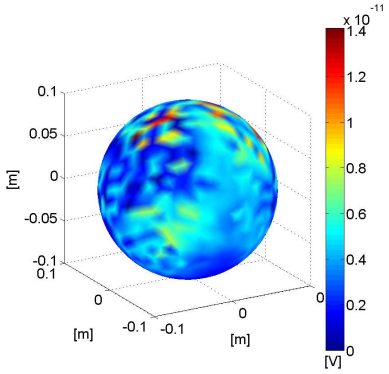

(e) MFS absolute error

FIG. 4.2. *Current dipole in a homogeneous sphere. Analytic solution, computed solution by BEM and MFS ($R_{MFS} = 0.8$) with 11995 collocation points or elements and respective error distributions.*

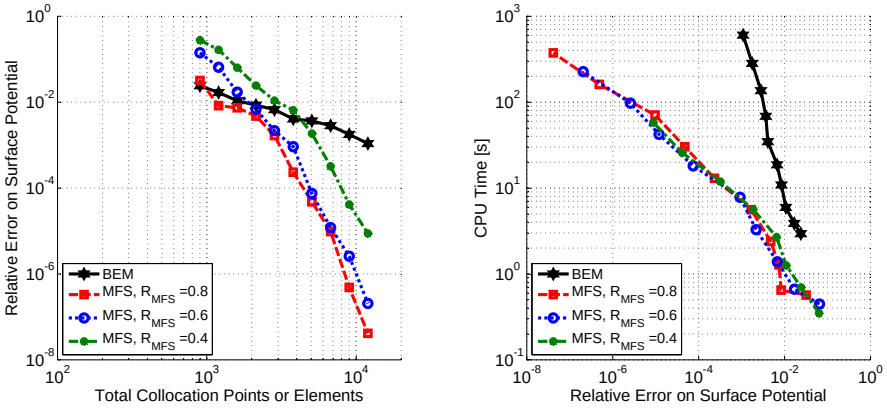

(a) Convergence (b) Cost per Accuracy

FIG. 4.3. *Dipole in a tree-layered sphere.*

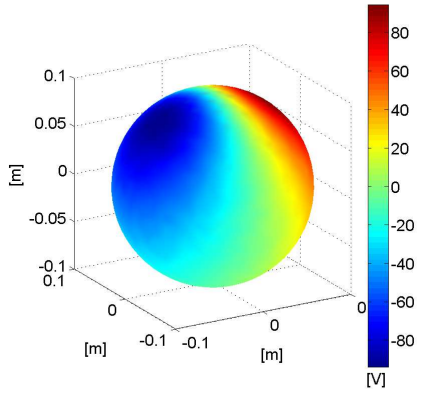

(a) Analytic surface potential

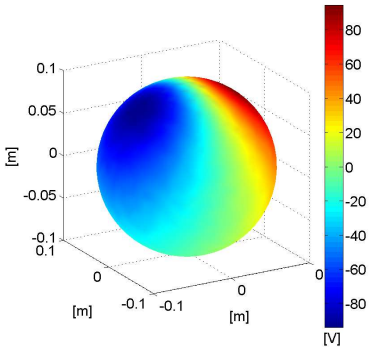

(b) BEM computed potential

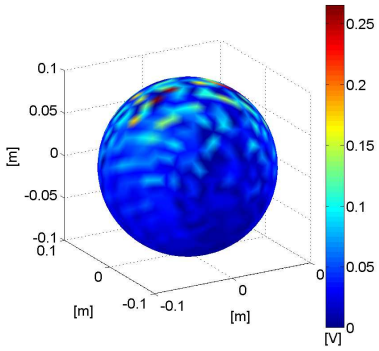

(c) BEM absolute error

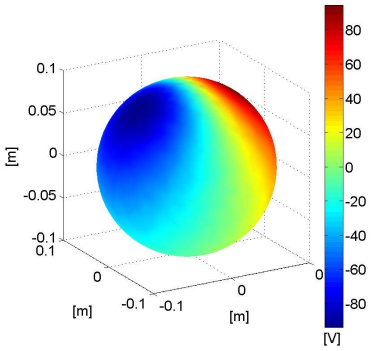

(d) MFS computed potential

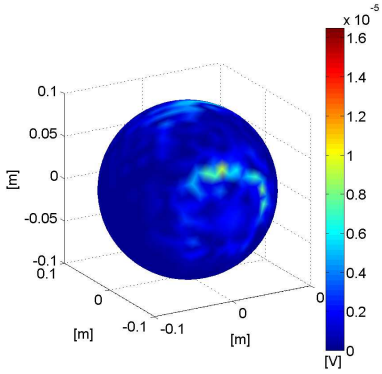

(e) MFS absolute error

FIG. 4.4. *Current dipole in a three-layered sphere. Analytic solution, computed solution by BEM and MFS ($R_{MFS} = 0.8$) with 11996 collocation points or elements and respective error distributions.*